Paleoclimate-induced stress on polar forested ecosystems prior to the Permian–Triassic mass extinction

Erik Gulbranson (erikgulbranson@gustavus.edu)
Gustavus Adolphus College https://orcid.org/0000-0003-1059-2938
Morgan Mellum
Gustavus Adolphus College
Valentina Corti
Università di Siena
Aidan Dahlseid
Gustavus Adolphus College
Brian Atkinson
University of Kansas
Patricia Ryberg
Park University
Gianluca Cornamusini
Università di Siena

Article

Keywords: end Permian extinction, dendrochronology, tree ring growth

Posted Date: December 1st, 2021

DOI: https://doi.org/10.21203/rs.3.rs-1108556/v1

Abstract

The end Permian extinction (EPE) has been considered to be contemporaneous on land and in the oceans. However, re-examined floristic records and new radiometric ages from Gondwana indicate a nuanced terrestrial ecosystem response to EPE global change. Paleosol geochemistry and climate simulations indicate paleoclimate change likely caused the demise of the widespread glossopterid ecosystems on Gondwana. Here, we evaluate the climate response of plants to the EPE via dendrochronology to produce annual-resolution records of tree ring growth for a succession of Late Permian and early Middle Triassic fossil forests from Antarctica. Paleosol geochemistry provides a broader context paleoclimate history. The plant responses to this paleoclimate change were accompanied by enhanced stress during the latest Permian. These results suggest that paleoclimate change during the Late Permian exerted significant stress on high-latitude forests, consistent with the hypothesis that climate change was likely the primary driver of the extinction of the glossopterid ecosystems.

Introduction

The end-Permian extinction (EPE) was one of the most severe mass extinctions in the history of metazoan life. The effects of the EPE were pronounced for marine organisms, including a nearly instantaneous (~30kyr) record of extinction in paleotropical seaways[1] that was coincident with a drastic reorganization of seawater chemistry and circulation[2]. It is surmised that terrestrial organisms underwent a similar and synchronous extinction[3], however, terrestrial flora and fauna during the Late Permian and the EPE display localized and asynchronous extinction and origination rates [4,5,6,7,8]. Of the plant lineages that did go extinct at the close of the Permian period, the most widespread were the glossopterids of Gondwana.

During the Late Permian, glossopterids occurred on every continental landmass of Gondwana, and were the predominant arborescent taxa of terrestrial ecosystems at paleo polar latitudes[9]. These plants were adapted for a broad range of climate conditions, changes of climate state (e.g., icehouse to greenhouse), and persisted as a low biodiversity floral province throughout the Permian[10]. It is, therefore, a paradox that such a cosmopolitan flora was unable to cope with global change during EPE. In Australia[4], glossopterids went extinct approximately 370 kyr prior to the marine EPE at 251.939±0.031 Ma[1], indicating that the specific mechanism(s) to stress these ecosystems differed in type, timing, or magnitude from the marine extinctions. How this array of climate and environmental change directly affected terrestrial ecosystems is a key area of research, but what is known is that ecosystem recovery was delayed, and taxa that filled-in ecosystem niches following the EPE were most likely affected by repeated environmental/climatic stress during the Early Triassic[11].

Recovery flora appear in the dispersed record in the Early Triassic and suggest a delayed recovery of paleo-equatorial ecosystems[12]. In Antarctica, however, there is a limited dispersed or megafloral record of

the Early Triassic, with putative leptosporangiate fern spores and megafloral fragments reported from the Allan Hills[13]. Megaflora of the early Middle Triassic, however, occur across Gondwana[5,14]. In Antarctica, the early Middle Triassic flora was highly diverse in comparison to the Permian counterpart[15] including: peltasperms, gingkophytes, corystosperms, conifers, and a higher diversity of understory vegetation (possibly including peltasperms). Depositional systems and soil-forming environments during the Middle Triassic were unlike those of the Late Permian[16,17]. In Antarctica, poorly developed soils that were likely waterlogged and wetlands that characterize the Late Permian[18] were replaced by deeply weathered soils, rich with soil-formed clay and oxide minerals in the Middle Triassic[16, 17].

What were the factors that led to the demise of the glossopterid ecosystems? Recent paleoclimate simulations and sediment geochemistry from eastern Australia postulate a climate-forced stress on plant growth via numerical paleoclimate simulations for the Bowen and Sydney basins[4,14,19]. Here, we test this hypothesis using dendrochronologic analysis of permineralized wood from the Shackleton Glacier area and Southern Victoria Land, Antarctica (Fig. 1). Both regions preserve paleo polar forested ecosystems in the Late Permian and early Middle Triassic. It is demonstrated here that just prior to the demise of the glossopterid floral province, a distinct change in paleoclimate had occurred, which resulted in greater stress on arborescent taxa. Moreover, the paleoclimate in the early Middle Triassic was similar to the latest Permian, however, the plant responses to this climate were markedly more amenable. This result stands in stark contrast to the earlier Late Permian record of plant-climate response, suggesting that by the latest Permian the polar forested ecosystems were in a state of disequilibrium, with plants failing to adapt to an ever-changing climate.

Geologic setting and age

Antarctica hosted several depositional basins that were actively subsiding during the late Paleozoic and early Mesozoic, of these the Transantarctic Basin was the largest (Fig. 1a). During the Permian–Triassic the Transantarctic Basin was situated close to the paleo south pole (Fig. 1b). The foreland-style basin preserves predominantly terrestrial strata with abundant plant fossils. Stratigraphic names and correlations are broadly subdivided into the central Transantarctic Mountains (CTAM) area and southern Victoria Land (SVL, Fig. 1a). Permian strata include the Buckley Fm. and Lower Fremouw Fm. (CTAM) and the Weller Coal Measures (SVL). Triassic strata include the Fremouw Fm. and Falla Fm. (CTAM) and the Feather Conglomerate and Lashly Fm. (SVL). In the CTAM area, *Protohaploxypinus microcorpus* has been recovered from the Upper Buckley Fm. at Graphite Peak below the first occurrence of *Lystrosaurus*[20], indicating a Changhsingian age; fossil wood with glossopterid affinities and *Vertebraria* at nearby Collinson Ridge and Shenk Peak were collected in the Lower Fremouw Fm. between 10–30 m, respectively, below the first occurrence of *Lystrosaurus* remains, indicating a Changhsingian age for these samples. A maximum depositional age of 253.5 ± 2.0 Ma from U-Pb analyses on zircon confirms a Late Permian age of the Buckley Fm. in the CTAM area[21]. Weller Coal Measures yield pollen and spore assemblages of the *Protohaploxypinus* Biozone and *Praecolpites sinuosus* consistent with a

Guadalupian to Lopingian age[22]. The Lashly A and B mbrs., the underlying Feather Conglomerate, and the Lower Fremouw Fm., yield palynomorphs of the *Aratisporites parvispinosus* Biozone and *Alisporites* Biozone, suggesting a late Early Triassic age[23]. The Lower Fremouw Fm. contains characteristic Early Triassic vertebrate fauna: *Thrinaxodon*, and *Lystrosaurus*, whereas the Upper Fremouw Fm. contains fossils of the *Cynognathus* C Biozone of the Karoo Basin, indicating an Anisian age for the Upper Fremouw Fm.[24] The vertebrate biostratigraphy and palynology all suggest a late Early (Olenekian) to early Middle (Anisian) Triassic age for these strata.

Results

Dendrochronology. Cross-matched tree ring widths (TRW) are converted to an index called the Ring Width Index (RWI), which evaluates the measured TRW in the sample against the expected TRW produced from a spline fitted to the data. Climate, being one of the state factors for tree growth, is anticipated to be a maximum signal in these RWI values due to principal of ecologic amplitude[25], where these trees grew at the limit of their natural range. To detect these signals in RWI time series we apply the technique of continuous wavelet transform (CWT) analysis to this data. One of the key visualizations of CWT results is in the form of a wavelet scalogram (Figs. 2g, 3, 4), which is a visualization of the Fourier period on the ordinate axis and the time dimension on the abscissa. The color map in the scalogram refers to the power (square of the wavelet coefficient) of the wavelet against the time series. The null hypothesis for this analysis is of a red noise spectrum, and regions at 0.05 significance level against the null hypothesis are illustrated by bold dark lines. The conical feature, determined by the e-folding time of the wavelet, in each scalogram reflects the region where edge-effects create spurious correlations. Replication of these dendrochronologic results is assessed by statistical comparison of two nearly identical TRW chronologies from the Lower Triassic Lashly Fm. using a cross-wavelet analysis (Figs. 2g,h). Statistics of inter-tree cross-matches are provided in Supplemental file 1 and are organized by the location of the samples used to develop each TRW chronology. As a supplement to this table the: 1) the chronology length; 2) subsample signal strength; and 3) distribution of anomalously wide/narrow rings are reported below.

The stratigraphically lowest samples reported here are from the Upper Buckley Formation, McIntyre Promontory. Eight cross-matched samples produce a chronology of 42 yrs. This chronology is ~2 $\log_2$ units less than the other data sets reported here, which indicates it has a shorter range of scales than the other chronologies (Fig. 2a). Thus, the decreased sample length inhibits comparisons of the longer periodicities extracted from the other chronologies reported here. However, the chronology is robust with a mean overlap of individual TRW records of 20 yrs. The mean correlation between radii of individual trees (intra-tree correlation) is better than 0.7, with percent parallel covariation better than 80%. The SSS cutoff of 0.5 is reached by year 22 of the 42 yr chronology. By comparison the TRW chronology from the Weller Coal Measures, Allan Hills, exceeded the SSS cutoff by year 26 of the 86 yr chronology (Fig. 2b). For the McIntyre Promontory chronology and the Weller Coal Measures, very narrow rings are well-correlated throughout the chronology, whereas anomalously wide rings correlate well, but are not well-expressed in

every sample. While not precisely correlated across the Transantarctic Basin, these fossil wood chronologies are both approximately 50 m below the lithostratigraphic contact between Upper Permian and Lower Triassic strata.

Individual fossil trees from Shenk Peak are associated with an intensely root-turbated paleosol preserving vertical to subvertical *Vertebraria* fossils. Fossil wood from Shenk Peak is stratigraphically higher than the samples from McIntyre Promontory, occurring within the lithostratigraphic division of the Lower Fremouw Fm.[20] Of the six samples measured, one did not produce a reliable cross-match due to limited overlap at either end of the chronology. The remaining five samples produce a chronology of 113 yrs. This chronology is within $\log_2$ dimensions of the: Allan Hills (Late Permian), Collinson Ridge (Late Permian), and Triassic chronologies; thus, producing meaningful comparisons of periodicity of RWI variation of these four TRW records (Fig. 2c). The mean correlation between radii of individual trees (intra-tree correlation) is better than 0.8, with percent parallel covariation better than 85%. The SSS cutoff of 0.5 is reached by year 35 of the 113 yr chronology. Very narrow rings that occur are exceptionally well-correlated with the exception of sample five at year 27 of the chronology. Unlike the stratigraphically lower chronologies, wide rings are well-correlated and expressed well in each sample.

Individual fossil trees from Collinson Ridge were sampled in the field as part of one of three *in situ* fossil forests in the Lower Fremouw Fm. The sampled fossil forest contains at least 27 *in situ* fossil trees interbedded with air-fall tuff and siltstones containing *Glossopteris* compressions/impressions and *Vertebraria* fossils. Seven measured samples produce a chronology of 176 yrs. The mean correlation between radii of individual trees (intra-tree correlation) is better than 0.75, with percent parallel covariation better than 80% (Fig. 2d). The SSS cutoff value of 0.5 is reached by year 55 of the 176 yr chronology, indicating a significant portion of the chronology preserves climate signals. Very narrow rings are very well-correlated, and wide rings are similarly correlated and expressed between different samples.

Triassic fossil wood was cross-matched from the Lashly B Fm., Allan Hills, SVL. The results of these cross-matches are reported elsewhere[17]. This data is used herein to make geospatial comparisons of Late Permian TRW chronologies in between the CTAM and SVL regions of Antarctica and for temporal comparisons from the Late Permian through the early Middle Triassic. Triassic fossil wood from the Allan Hills resulted in a 238 yr chronology exclusively from transported fossil wood. Triassic fossil wood reaches the 0.5 SSS cutoff at year 30 of the 238 yr chronology, yielding a long-lived record of paleoclimate history (Fig. 2e). Narrow rings are well-correlated, and wide rings are correlated with the exception of sample one between years 25–30 of the chronology.

Reproducibility of dendrochronologic results. The cross-wavelet power spectrum applied to the two independently sampled and measured Triassic TRW chronologies (ELG and VC) produces significant power (0.05 significance level) for Fourier periods ranging from 14–16 yrs and 20–64 yrs, with negative correlations existing for Fourier periods 14–16 yrs and positive correlations for Fourier periods 16 yr and 32 yr (Fig. 2g). Wavelet coherence, analogous to a correlation coefficient ranging from 0–1, is significant at the 0.05 level for Fourier periods 3–4 yrs, 10 yr, and 32 yr (Fig. 2h). Average coherence values are better

than 0.85 for the higher frequency signals, and better than 0.95 for the lower frequency signals. The phase is complex for higher frequencies, displaying both lag/lead patterns and positive/negative correlations with respect to time. However, the phase is more organized at lower frequencies with either the ELG chronology lagging behind the VC chronology, or positive correlation between the two chronologies. The range of Fourier periods with significant cross-wavelet power and wavelet coherence are identical to the significant Fourier periods identified in each chronology individually using CWT analysis (Fig. 3e,f), with 0.95 average wavelet coherence for the prominent lower frequency signals in both TRW chronologies.

Continuous Wavelet Transform. CWT results for the lowest stratigraphic position of Late Permian fossil wood (Upper Buckley Fm., McIntyre Promontory; Weller Coal Measures, Allan Hills) indicate a lack of Fourier periods >20 yrs, with significant signals at the 2 yr, 3–5 yrs, and 9–15 yrs (Figs. 3a,b). The higher frequency signals are not consistent over the length of the chronology, however, the shorter frequency signals are more consistent. For the stratigraphically highest Late Permian fossil wood samples (Lower Fremouw Fm., Shenk Peak; Collinson Ridge) there is a similar range of high frequency signals as for the stratigraphically lower samples, however, there is an emergence of prominent Fourier periods in the 20–30 yr range that are continuous or more frequently occurring throughout a chronology (Figs. 3c,d). The Collinson Ridge chronology displays a marked lack of significant high frequency signals for nearly a century, with high frequency signals occurring over ~50 yr durations on either end of the chronology. The Triassic chronologies (Allan Hills) display intermittent high frequency signals and more persistent periodicities in the 15–30 yrs range, with potentially minor contributions of periods in the ~50 yr range (Figs. 3e,f).

Geochemistry. Long-term paleoclimate averages from the sedimentary record are developed here across for Upper Permian and Lower Triassic strata. Comparisons of reconstructed paleoclimates are made between the well-studied Sydney and Bowen basins[4,19,] and the study area of the Transantarctic Basin[18]. Sediment geochemistry data from the Bowen and Sydney basins[19] is correlated between several cores and averaged to produce a summary of temporal trends in chemical weathering. The paleo land surface temperature (LST) is reconstructed via linear relationship with the chemical index of alteration (Fig. 3g). Paleosol geochemistry from Graphite Peak, Transantarctic Basin[18] was converted to the K-corrected chemical index of alteration and LSTs were estimated from this data (Fig. 3g). The two stratigraphic records of LSTs produce differing magnitudes of variation over time, with the Sydney and Bowen basins preserving a more gradual change per unit time, but with clear oscillations (Fig. 3g). In contrast, the paleosol results from Graphite Peak display large variations in LST estimates. However, both study areas produce similar long-term trends in paleo-LST, with: 1) a >10ºC warming during the Late Permian; and 2) identical temperatures that remain constant across the Permian–Triassic boundary. The Early–Middle Triassic results, however, indicate remarkable differences between each area in paleo-LST variance through time (Fig. 3g).

A well-developed early Middle Triassic paleosol from the Allan Hills is studied in detail for paleo soil-forming processes and geochemistry (supplemental files 1, 4). Major element abundances of the Triassic

paleosol display down-profile trends of Ca, Mn, Al, K, and Mg, with slightly variable Na abundance. The abundance of Mn is depleted in the B horizons but highly abundant in the parent material where Mn-nodules were observed in the field. The abundance of Ca is notably depleted in the B horizons of this paleosol relative to the parent material; whereas Al, K, and Mg are abundant in the B horizons and display a gradual decline towards the parent material. For application of paleoclimate proxies the CIA-K value maintains a >5% difference between the parent material and overlying B horizons, indicating the likelihood that the geochemical effects of soil-forming processes are preserved in this paleosol.

Discussion

The data presented here provides direct evidence of the response of plants to climate in the Late Permian and early Middle Triassic. For context, the Late Permian ecosystems of Antarctica were low diversity forests with arborescent taxa dominated by the glossopterids. Despite low generic diversity, however, isotopic data indicate varied functional diversity of glossopterids in the form of leaf habit[27] and likely a greater speciation of glossopterids based on their reproductive organs[28]. These ecosystems were long-lived on Gondwana[9,10], forming the predominant vegetative cover for the Permian after the end of the late Paleozoic ice age. Following the Late Permian, evidence from the Sydney and Bowen basins indicate prolonged environmental disturbance resulting in the predominance of toxic algal blooms in freshwater settings[29]. The ecologic recovery from this disturbance in early Middle Triassic preserves a much higher diversity of arborescent and herbaceous vegetation[15], with the re-emergence of pteridosperms in the Transantarctic basin in the form of *Dicroidium* and associated corystosperm wood morphogenera[30]. The paleoclimate change accompanying these ecologic shifts is discussed here in two temporal scales and over a range of paleolatitude. Long-term paleoclimate change is inferred from the Sydney, Bowen, and Transantarctic basins through analysis of major element concentrations in sedimentary rocks and paleosols[18,19]. The dendrochronology data herein provides “snapshots” on a centennial timescale for the organismal response to paleoclimate at a given time interval. Broad comparisons between low-latitude and high-latitude climate are addressed through comparison of eastern Pangea successions of sedimentary rocks and paleosols[31,32,33] to the aforementioned strata.

What were the specific changes to paleoclimate? Changes in atmospheric circulation and humidity likely explain the long-term paleoclimate averages of sediment geochemistry data[19]. The paleosol geochemistry data (Fig. 4e) presented herein confirms that assessment, for long-term averaging of paleoclimate information. However, the dendrochronology data herein is presented at annual resolution, which has the potential to highlight specific climate change mechanisms. Without suitable comparison to annually-resolved paleoclimate simulations it is speculated that oscillatory phenomena such as the extant Arctic annular oscillation (AO) is a plausible atmospheric–surface ocean modern analogue that may explain some of the oscillatory behavior observed in the deep time tree ring chronologies. Given that AO, like our CWT results, is non-stationary and does not occur at a fixed periodicity and occurs at high-latitudes. However, the uncertainty of specific climate change mechanisms despite having robust

annually-resolved paleoclimate records underscore the need for higher-resolution paleoclimate simulations to compare to this new tool for deep time paleoclimate research.

The CWT analysis presented here uses the Morlet wavelet (Fig. 3a–f), which is useful for detecting oscillatory signals and their stationarity in a time series. However, because the Morlet wavelet uses real and imaginary numbers, the wavelet power includes information about amplitude and phase, hence resolution at fine-time scales is sacrificed for accuracy of the frequency domain[26]. By selecting a derivative of a gaussian wavelet (DOG, 2nd order derivative), the resolution of the time scale conforms to the resolution of the original data set, due to visualizing positive and negative oscillations as separate peaks, allowing for direct comparison to be made of wavelet coefficients to the RWI for a given year (Fig. 4a–d). Of the growth years that correlate to significant wavelet coefficients in the latest Permian chronologies, 60-62% correspond to years of suppressed growth, mostly around the 30 yr periodicity. In contrast, only 40% of the growth years in the early Middle Triassic correspond to suppressed growth, also mostly around the 30 yr periodicity. Thus, despite similar patterns of oscillatory paleoclimate in the latest Permian and early Middle Triassic, the plant communities responded in vastly different ways to this climate state, with the latest Permian glossopterid forests being indicative of a highly stressed ecosystem.

Longer-term averages of paleoclimate information are derived from the morphologic and geochemical analysis of paleosols and sedimentary rocks (Figs. 3g, 4e)[18,19,31–33]. The Late Permian witnessed an increase in land surface temperatures (LSTs) by 10ºC or more[19], consistent between eastern Australia, Antarctica. However, the paleotropical North China craton sedimentary record shows a comparatively muted temperature increase of ~5ºC[31] (Fig. 3g). A brief time interval across the Permian–Triassic boundary, however, was markedly devoid of LST variation in all areas. Moreover, paleosol geochemistry from previous studies[16,18,34], when applied to a paleoclimate proxy[35], indicate that Late Permian paleoclimate established a humidity gradient between SVL and CTAM (Fig. 4e). These results stand in stark contrast to the overwhelming evidence for aridification in the paleotropical latitudes during the Late Permian[31–33], indicating that while the evidence for warming is consistent for terrestrial and marine strata, the effect on climate was likely related to zonal patterns in atmospheric/surface ocean circulation. The results of paleosol geochemistry for this study indicate that the early Middle Triassic paleosol from the Allan Hills formed under a humid and afforested biome, consistent with the production of clay and Fe-oxide minerals in the studied profile. However, by the latest Permian and to the early Middle Triassic both SVL and CTAM paleosols converge to the same humidity and floral province biome as the paleosol studied herein. These results are consistent with the interpretations of the dendrochronology time series, where distinct changes in oscillatory behavior are observed to coincide with prominent shifts in LST during the Late Permian, where the Middle Triassic displays an overall similar paleoclimate in the study region.

The Sydney and Bowen basins were adjacent to the study area during the Late Permian–Middle Triassic. Recently it has been hypothesized that terrestrial ecosystems underwent an ecologic collapse prior to the

marine-defined EPE[4,36], and that paleoclimate was likely the driver of ecosystem collapse and restructuring[14,19,29]. Based on this hypothesis it would be expected that contiguous ecosystems at higher paleolatitudes would be equally sensitive to the same climate forcing. This study, therefore, evaluates this hypothesis through the record of paleoclimate change in the plants that went extinct during the Late Permian. The shift in periodicity of climate signals from the Late Permian to latest Permian fossil wood confirms a climate change event during the time interval preceding ecosystem collapse at the paleo high-latitudes. Moreover, the correlation of this 30 yr oscillation with years of suppressed growth in the Permian, in contrast with correlated enhanced growth in the Triassic, further supports the implication that specific changes in Late Permian paleoclimate were deleterious to terrestrial ecosystems on Gondwana.

Conclusions

This study documents the history of tree ring growth at paleo polar latitudes from the Late Permian–early Middle Triassic in order to evaluate the hypothesis that paleoclimate change was a principal cause of the demise of glossopterid ecosystems. Dendrochronologic results are statistically robust and highlight a change in the period and stationarity of oscillatory climate effects on tree ring growth in the study area. Geospatial comparisons of dendrochronologic results indicate a subtle gradient existed between the two study regions, with the gradient decreasing into the early Middle Triassic, consistent with long-term averages of paleoclimate derived from paleosol climate proxies. Latest Permian tree ring chronologies are markedly similar to the early Middle Triassic chronologies, with a key difference being the correlation of a 30 yr signal with years of reduced growth for Permian trees and a correlation of a 30 yr signal with years of enhanced growth for Triassic trees. These results add support to the hypothesis that paleoclimate exerted significant stress to terrestrial ecosystems during the Late Permian and that these stressors occurred in advance of the marine record of the end Permian extinction.

Methods

Study sites. The fossil wood used in this study was collected from Permian and Triassic strata of the Transantarctic Basin in the CTAM and SVL regions of Antarctica. Late Permian fossil wood was collected from the Upper Buckley Fm. at McIntyre Promontory (CTAM, S84°55.168', E179°43.182'). Fossil wood stratigraphically close to the Permian–Triassic transition was collected from the Lower Fremouw Fm. at Shenk Peak and at Collinson Ridge (CTAM, S85°13.275', W173°57.704'; S85°20.051', W175°28.218', respectively). Of these samples, only fossil wood at Collinson Ridge is preserved as *in situ* fragments. The remaining wood samples are preserved as horizontal to subhorizontal wood fragments in sandstone/siltstone strata. Fossil wood material was collected from specimens where >20 growth rings can be identified, a minimum number of rings for replicable cross-dating. Comparisons are made to previous dendrochronologic results from the Permian Weller Coal Measures (S76°42.577', E159°42.826') and Triassic Lashly Fm. (S76°40.524', E159°52.203'), Allan Hills (SVL,[17]).

Paleobotany. Tree rings identified in hand sample are cross-referenced to thin-sections of the transverse and radial planes of fossil wood. The taxa studied include glossopterid wood from Upper Permian

successions in CTAM and SVL, which are dominated by woody axes with affinity to the glossopterids, and are associated with megafloral remains of *Glossopteris* leaves, *Vertebraria* roots, and reproductive organs related to the glossopterids[37]. The Permian fossil wood studied herein preserves elements of wood anatomy consistent with wood morphogenera associated with the glossopterids. The early Middle Triassic, however, contains a more diverse megafloral community of arborescent plants. Distinguishing wood morphogenera between conifers and corystosperms is challenging due to the conservative nature and few unique properties to distinguish these taxa[30]. However, while not conclusive, the early Middle Triassic wood studied herein was collected from sedimentary beds containing an abundance of *Dicroidium* leaf compressions and the woody axes display the prominent lobed property associated with corystosperm fossil wood. It should be noted, however, that highly diverse leaf megafossil assemblages containing conifers, ginkgophytes, and peltasperms are present in this succession of strata.

Dendrochronology. The techniques of dendrochronology (statistical cross-matching of tree ring widths, TRW) have been successfully applied to fossil wood material in deep time in order to generate robust annual chronologies of wood growth [17,38,39,40]. Here, these techniques are applied to Permian and Triassic fossil wood to study the paleoclimate history during the time of this wood growth. As climate is among the most important state factors for tree growth[25], and that these extinct trees grew near the limit of their natural range, it is expected that paleoclimate information is encoded in the TRW variation of these samples. Thin sections of the transverse and radial planes were made from each sample to assess the preservation state of the fossil wood material; and relate the anatomically defined ring boundaries to their macroscopic expression in hand sample. TRWs were measured by hand with high-precision calipers under 10x magnification. For each sample a minimum of two radial transects were measured to ensure replication of the TRW measurements. Several samples were measured independently by two to three analysts. Cross-matching was performed using PAST5™ software on: replicate TRW transects of a sample (intra-tree cross-matching); and between different samples (inter-tree cross-matching). Intra-tree and inter-tree cross-matching was assessed via statistical comparison of: 1) t-statistics (T_{BP}[41]; T_{HO}[42]); 2) the correlation coefficient; and 3) percent parallel covariation. Additional considerations on accepting or rejecting a cross-match include: 1) the number of overlapping rings; 2) the number of inter-tree cross-matched samples at unit chronology length (sample depth); and 3) anatomical constraints on internal cross-matching. Detrending of the raw TRW data to remove spurious growth-related trends in TRW was performed with a smoothing spline. The detrended master TRW chronology is converted to the Ring Width Index (RWI), which is an index relating the measured TRW to the expected TRW for a given ring number. RWIs have a value that is either <1 (less growth than expected), =1 (expected growth), or >1 (more growth than expected). The potential that a segment of a chronology preserves the total expression of a climate signal in a TRW chronology is assessed statistically via the subsample signal strength (SSS) with dplR in R[43] with a cutoff value of 0.5 arbitrarily chosen to represent robust inter-series correlations[44].

Continuous wavelet transform. Given that annually-resolved meteorologic variation in deep time is not widely reported, and that the studied taxa are extinct with no viable modern counterpart for comparison,

the periodicity of RWI variation via continuous wavelet analysis is used to infer the response of the studied fossil wood to oscillatory paleoclimate variation. However, each RWI chronology must have a Gaussian distribution in order to be used in a continuous wavelet transform (CWT). Probability plots (supplementary figure 1) of RWI chronologies are used to determine the type of statistical distribution the data has prior to CWT. A CWT decomposes a time series to provide information about specific frequencies, their variation through time, and significance level[26]. The Morlet wavelet was selected as an appropriate choice due to its: 1) simplicity; 2) widespread use; and 3) that it contains real and imaginary values for phase and amplitude comparisons[26]. Significance tests of the resulting wavelet power spectra were performed in R using the dplR[43], and Wavelet Comp packages[45]. Significance tests evaluate wavelet power against the null hypothesis of a background spectrum of red noise, produced via an autoregressive process. Wavelet power that exceeds the red noise spectrum at the 5% significance level is interpreted to be a true feature of the data. Wavelet scalograms (Figs. 3a–d, 4b,d) were produced in Mathematica.

Reproducibility. CWT results from two independently measured (by ELG and VC) TRW chronologies from the Triassic Lashly B Formation, Allan Hills (SVL) are compared via the technique of cross-wavelet transform to produce the cross-wavelet power spectrum and wavelet coherence[26]. This technique is applied here, via the Wavelet Comp package in R, to evaluate how reproducible TRW chronologies are in deep time as the fossil wood for both chronologies was sampled from closely spaced locations on two vertically associated bedding planes in the Lashly Fm. in the Allan Hills. Thus, while minor differences are expected, the closely spaced nature of these samples in the sedimentary strata suggest a similar distribution of TRW signals should result, without the potential to provide meaningful cross-matches. The cross-wavelet power spectrum provides information about covariance at each unit time between two time series, with higher cross-wavelet power indicating a common power between the two time-series. Whereas the wavelet coherence provides information on the correlation of two time series per unit time, regardless of the power, providing information on how well-correlated two time series are. Coherence values approaching 0 indicate poor correlation, and coherence values approaching 1 indicate high correlation at the specified significance level. The phase of the covariance is reported for the cross-wavelet power spectrum and the wavelet coherence to inspect whether a correlation is positive or negative or whether one time series leads the other.

Paleosol geochemistry. Paleosol morphology and major element geochemistry are used to provide an independent assessment of paleoclimate in the study region from the Permian and Triassic. Paleo rainfall estimates are derived from the CIA-K proxy[46], and paleohumidity and floral province inferences are derived from a separate proxy[35]. For this study major element geochemistry is reported from a well-developed gleyed ferritic Argillisol (iron- and clay-bearing paleosol with a prominent zone of reduced or oxidized material) profile that was described and sampled in the Lashly A Fm., Allan Hills (SVL)[17]. Paleosol morphology was described in the field at the cm-scale, and representative samples of the five identified subsurface horizons and parent material were collected. A bulk subsample from each horizon was ground, homogenized via mixing, fused with Li-metaborate, and dissolved in 6N HCl. 20-fold diluted aliquots were analyzed by ICP-MS (Agilent 7700) at Gustavus Adolphus College (USA) for Al, Ca, Mg, Na,

Mn, and K. Elemental abundances are converted from weight percent to moles for use in the paleoclimate proxies. Published paleosol morphology and geochemistry[16,18,34] from the Permian and Triassic of CTAM and SVL are used to provide a complete and comparable paleosol-derived paleoclimate record in the study area.

References

[1]Shen, S.-Z., et al. A sudden end-Permian mass extinction in South China. *GSA Bulletin* **131** (1-2), 205–223, doi: https://doi.org/10.1130/B31909.1 (2019).

[2]Rampino, M.R., Caldeira, K. Major perturbation of ocean chemistry and a 'Strangelove Ocean' after the end-Permian mass extinction. *Terra Nova* **17**, 554–559, https://doi.org/10.1111/j.1365-3121.2005.00648.x (2005).

[3]Cascales-Miñana, B., Cleal, C. The plant fossil record reflects just two great extinction events. *Terra Nova* **26**, 195–200 (2014).

[4]Fielding, C.R., et al. Age and pattern of the southern high-latitude continental end-Permian extinction constrained by multiproxy analysis, *Nat. Comm.* **10**, 385 (2019).

[5]Nowak, H., Schneebeli-Hermann, E., Kustatscher, E. No mass extinction for land plants at the Permian-Triassic transition. *Nat. Comm.* **10**, 384, doi: https://doi.org/10.1038/s41467-018-07945-w (2019).

[6]Gastaldo, R.A., Neveling, J., Geissman, J.W., Kamo, S.L., Looy, C.V. A tale of two Tweefonteins: What physical correlation, geochronology, magnetic polarity stratigraphy, and palynology reveal about the end-Permian terrestrial extinction paradigm in South Africa. *GSA Bulletin* doi: https://doi.org/10.1130/B35830.1 (2021).

[7]Xiong, C, Wang Q. Permian–Triassic land-plant diversity in South China: Was there a mass extinction at the Permian/Triassic boundary? *Paleobiology* **37.1**, 157–167 (2011).

[8]Feng, Z., et al. From rainforest to herbland: New insights into land plant responses to the end-Permian mass extinction. *Earth-Science Reviews* **204**, 103153 (2020).

[9]McLoughlin, S. Glossopteris–insights into the architecture and relationships of an iconic Permian Gondwanan plant. *Journal of the Botanical Society of Bengal* **65**, 93–106 (2011).

[10]Rigby, J.F. The Gondwana palaeobotanical province at the end of the Palaeozoic in 24th International Geological Congress (Montreal, 1972), Proceedings, Section 7, 324–330 (International Geological Congress, 1972).

[11]Retallack, G.J., et al. Multiple Early Triassic greenhouse crises impeded recovery from Late Permian mass extinction. *Palaeogeography, Palaeoclimatology, Palaeoecology* **308**, 233–251 (2011).

[12]Looy, C.V., Brugman, W.A., Dilcher, D.L., Visscher, H. The delayed resurgence of equatorial forests after the Permian–Triassic ecologic crisis. *PNAS* **96**, 13857–13862 (1999).

[13]Gabites, H.I. Triassic paleoecology of the Lashly Formation, Transantarctic Mountains, Antarctica. M. Sc. Thesis, 1–148 (Victoria University of Wellington, New Zealand, 1985).

[14]Mays, C., et al. Refined Permian–Triassic floristic timeline reveals early collapse and delayed recovery of south polar terrestrial ecosystems. *GSA Bulletin*, doi: https://doi.org/10.1130/B35355.1 (2019).

[15]Escapa, I.H., et al. Triassic floras of Antarctica: plant diversity and distribution in high paleolatitude communities. *Palaios* **26**, 522–544 (2011).

[16]Retallack, G.J., Krull, E.S. Landscape ecological shift at the Permian–Triassic boundary in Antarctica. *Australian Journal of Earth Sciences* **46**, 785–812 (1999).

[17]Gulbranson, E.L., Cornamusini, G., Ryberg, P.E., Corti, V. When does large woody debris influence ancient rivers? Dendrochronology applications in the Permian and Triassic, Antarctica. *Palaeogeography, Palaeoclimatology, Palaeoecology* **541**, 109544 (2020).

[18]Sheldon, N.D. Abrupt chemical weathering increase across the Permian-Triassic boundary. *Palaeogeography, Palaeoclimatology, Palaeoecology* **231**, 315–321 (2006).

[19]Frank, T.D., et al. Pace, magnitude, and nature of terrestrial climate change through the end-Permian extinction in southeastern Gondwana. *Geology*, doi: https://doi.org/10.1130/G48795.1 (2021).

[20]Collinson, J.W., Hammer, W.R., Askin, R.A., Elliot, D.H. Permian-Triassic boundary in the central Transantarctic Mountains, Antarctica. *GSA Bulletin* **118**, 747–763 (2006).

[21]Elliot, D.H., Fanning, C.M., Isbell, J.L., Hulett, S.R.W. The Permo-Triassic Gondwana sequence, central Transantarctic Mountains, Antarctica: Zircon geochronology, provenance, and basin evolution. *Geosphere* **13**, 155–178 (2017).

[22]Askin, R.A. Permian palynomorphs from southern Victoria Land, Antarctica. *Antarctic Journal of the U.S.* **30**, 47–48 (1995).

[23]Kyle, R.A., Schopf, J.M., 1982, Permian and Triassic palynostratigraphy of the Victoria Group, Transantarctic Mountains in Antarctic Geosciences (ed. Craddock, C.) 649–659 (University of Wisconsin Press, 1982).

[24]Sidor, C.A., Smith, R.M.H., Huttenlocker, A.K., Peecook, B.R. New Middle Triassic tetrapods from the Upper Fremouw Formation of Antarctica and their depositional setting. *Journal of Vertebrate Paleontology* **34**, 793–801 (2014).

[25]Fritts, H.C. Tree Rings and Climate (Academic Press, 1976).

[26]Torrence, C., Compo, G.P. A practical guide to wavelet analysis. *Bulletin of the American Meteorological Society* **79**, 61–78 (1998).

[27]Gulbranson, E.L., et al. Leaf habit of Late Permian Glossopteris trees from high palaeolatitude forests. *Journal of the Geological Society* **171**, 493–507 (2014).

[28]Ryberg, P.E. Reproductive diversity of Antarctic glossopterid seed ferns. *Review of Palaeobotany and Palynology* **158**, 167–179 (2009).

[29]Mays, C., et al. Lethal microbial blooms delayed freshwater ecosystem recovery following the end-Permian extinction. *Nat. Commun.* **12**, 5511 https://doi.org/10.1038/s41467-021-25711-3

(2021).

[30]Decombeix, A-.L., Bomfleur, B., Taylor, E.L., Taylor, T.N. New insights into the anatomy, development, and affinities of corystosperm trees from the Triassic of Antarctica. *Review of Palaeobotany and Palynology* **203**, 22–34 (2014).

[31]Lu, J., Zhang, P., Yang, M., Shao, L., Hilton, J. Continental records of organic carbon isotopic composition ($d^{13}C_{org}$), weathering, paleoclimate and wildfire linked to the End-Permian Mass Extinction. *Chemical Geology* **558**, 119764 (2020).

[32]Cui, C., Cao, C. Increased aridity across the Permian–Triassic transition in the mid-latitude NE Pangea. *Geological Journal*, https://doi.org/10.1002/gj.4123 (2021).

[33]Yu, Y., Chu, D., Song, H., Guo, W., Tong, J. Latest Permian–Early Triassic paleoclimatic reconstruction by sedimentary and isotopic analyses of paleosols from the Schichuanhe section in central North China Basin. *Palaeogeography, Palaeoclimatology, Palaeoecology* **585**, 110726 (2022).

[34]Sheldon, N.D., Chakrabarti, R., Retallack, G.J., Smith, R.M.H. Contrasting geochemical signatures on land from the Middle to Late Permian extinction events. *Sedimentology* **61**, 1812-1829 (2014).

[35]Gulbranson, E.L., Montañez, I.P., Tabor, N.J. A proxy for humidity and floral province from paleosols. *The Journal of Geology* **119**, 559–573 (2011).

[36]Vajda, V., et al. End-Permian (252 Mya) deforestation, wildfires and flooding–An ancient biotic crisis with lessons for the present. *Earth and Planetary Science Letters* **529**, 115875 (2020).

[37]Francis, J.E., Woolfe, K.J., Arnott, M.J, Barrett, P.J. Permian climates of the southern margin of Pangea: evidence from fossil wood of Antarctica in Pangea: Global Environments and Resources (eds. Embry, A.F., Beauchamp, B., Glass, D.J.) 275–282 (AAPG Memoir 17, 1994).

[38]Wright, W.E., Baisan, C., Streck, M., Wright, W.W., Szejner, P. Dendrochronology and middle Miocene petrified oak: Modern counterparts and interpretation. *Palaeogeography, Palaeoclimatology, Palaeoecology* **445**, 38–49 (2016).

[39]Luthardt, L., Rößler, R. Fossil forest reveals sunspot activity in the early Permian. *Geology* **45**, 279–282 (2017).

[40]St. George, S, Telford, R.J. Fossil forest reveals sunspot activity in the Early Permian: COMMENT. *Geology* **45**, e427 (2017).

[41]Baillie, M.G.L., Pilcher, J.R. A simple cross-dating program for tree-ring research. *Tree-Ring Bulletin* **33**, 7–14 (1973).

[42]Hollstein, E. Mitteleuropäische eichenchronologie, Trierer Grabungen und Forschungen XI, Philip von Zabern (1980).

[43]Bunn, A.G. Statistical and visual crossdating in R using the dplR library. *Dendrochronologia* **28,** 251–258, doi: 10.1016/j.dendro.2009.12.001 (2010).

[44]Buras, A. A comment on the expressed population signal. *Dendrochronologia* **44**, 130–132 (2017).

[45]Roesch, A., Schmidbauer, H. WaveletComp Computational Wavelet Analysis https://CRAN.R-project.org/package=WaveletComp. R package version 1.1 (2018).

[46]Sheldon, N.D., Retallack, G.J., Tenaka, S. Geochemical climofunctions from North American soils and application to paleosols across the Eocene-Oligocene boundary in Oregon. *The Journal of Geology* **110**, 687–696 (2002).

[47]Yang, J., Cawood, P.A., Du, Y., Feng, B., Yan, J. Global continental weathering trends across the Early Permian glacial to postglacial transition: correlating high- and low-paleolatitude sedimentary records. *Geology* **42**, 835–838 (2014).

[48]Panahi, A., Young, G.M., Rainbird, R.H. Behavior of major and trace elements (including REE) during Paleoproterozoci pedogenesis and diagenetic alteration of an Archean granite near Ville Marie, Québec, Canada. *Geochimica et Cosmochimica Acta* **64**, 2199–2220 (2000).

Declarations

Acknowledgements

This research was supported by National Science Foundation grants OPP 1443557 and OPP 1142749 to ELG, and grant OPP 1142495 to PER.

Author contributions

ELG, PER, BAA, and GC performed field investigations of Upper Permian and Lower Triassic strata in the field area, including sample collections and descriptions. ELG, MMM, VC, and AD contributed to the dendrochronology; ELG and VC performed the reproducibility test; ELG and MMM performed the

geochemical measurement and analysis; and ELG performed the CWT analysis and cross-wavelet transform. ELG assembled the manuscript and all authors contributed to the manuscript revision.

Competing interests

The authors declare no competing interests.

Figures

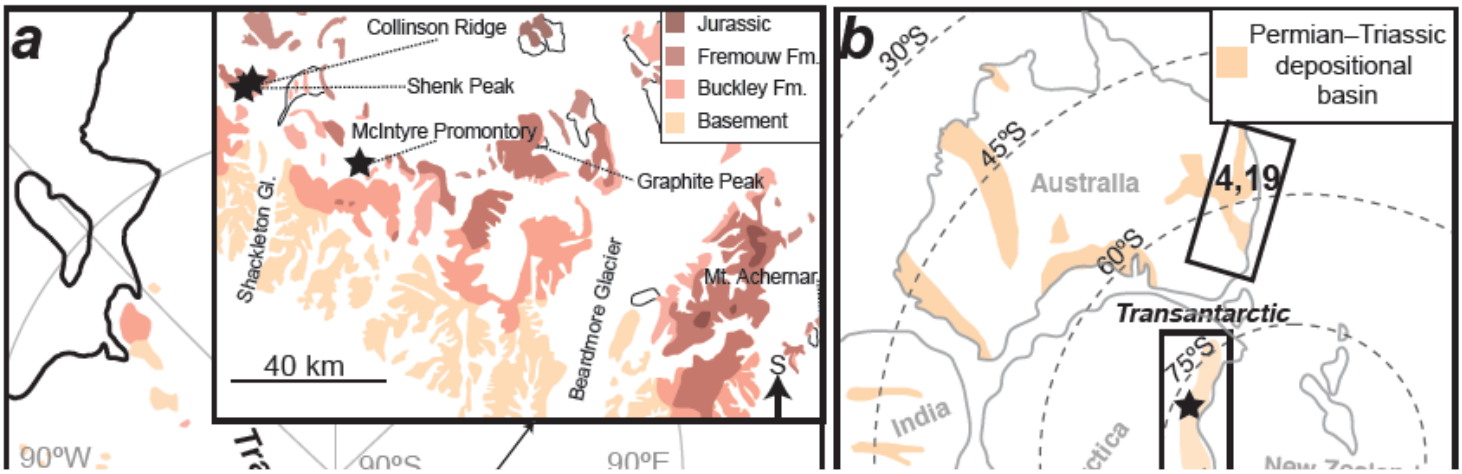

Figure 1

Map and paleogeography of the study area. a) Map of the study locations, CTAM and SVL, on Antarctica. Outcroppings of major geologic units are shown, ice/snow where not shaded. b) Paleogeographic reconstruction of the Late Permian for Gondwana. Permian–Triassic depositional basins are shaded, study locations indicated by stars. The boxed region of eastern Australia highlights the correlative stratigraphy discussed in the text4,19.

Figure 2

Ring width index (RWI) and correlation of the replicate early Middle Triassic chronologies (g–h). a–f), RWI plots of cross-matched tree ring width data. g) Wavelet scalogram of wavelet coherence between the two replicate Triassic chronologies: color spectrum is equivalent to the correlation of the two chronologies (0–1); the arrows indicate positive (pointing right) or negative correlation (pointing left); the up/down direction of arrows indicates if one chronology leads/lags another, respectively (irrelevant for this analysis as the two chronologies are not cross-matched to each other); white lines indicate the 0.05 significance level of wavelet coherence. h) Fourier period versus average wavelet coherence, the red dots signify Fourier periods significant at the 0.05 level for the specified wavelet correlation between the two chronologies.

Figure 3

Wavelet scalograms of the RWI data and land surface temperature (LST). a–f) The color spectrum indicates wavelet power (square of wavelet coefficient), higher power indicating a stronger signal in the data. The shaded envelope is the cone of influence reflecting wavelet coefficients that are erroneous near the edge of each time series. The dark lines indicate the wavelet power domains that are significant as compared to red noise at the 0.05 level. The abscissa represents the time represented in each chronology and is directly related to the RWI data. The ordinate axis represents the Fourier period and is scaled with 16 voices per octave. g) LST through time in Antarctica (dashed line and dashed circles)18, eastern Australia19 (solid line and filled circles), and North China31 (solid line and filled squares). Purple colors indicate Triassic data, and red colors indicate Permian data. LST estimates are based on the chemical index of alteration (CIA)47 and are corrected for authigenic K concentrations19,48. Data for eastern Australia represent sedimentary CIA values, and are averaged between the Bowen and Sydney basins based on existing correlations and U-Pb ages19. Data for Antarctica is from Graphite Peak and represent paleosol CIA values18. Markers indicating the last occurrence Glossopteris fossils are shown for Antarctica20 and eastern Australia4,19. The detrital zircon U-Pb for Antarctica is from Layman Peak in the Shackleton Glacier area21.

Figure 4

Tree growth patterns and paleoclimate. a–b) RWI and CWT analysis with the derivative of a gaussian (DOG, 2nd derivative) wavelet for the Late Permian Collinson Ridge chronology. c–d) RWI and CWT analysis via the DOG wavelet for the Triassic Allan Hills chronology. Intervals of reduced/enhanced growth as determined by RWI that correlate with significant wavelet coefficients are illustrated by the shaded vertical bars. e) Paleoclimate model results from paleosol geochemistry at each area in the study region from the Permian–Triassic, ET= evapotranspiration, Eppt=energy from precipitation, where these parameters are calculated from the equations for paleosol-based paleoclimate proxies35,46. Humidity provinces and floral regimes fall between each of the lines, and the calculated ET and Eppt values from each paleosol are shown by the symbols.

Supplementary Files

This is a list of supplementary files associated with this preprint. Click to download.

- Supplementalfile1.docx
- Supplementalfile2.xlsx
- Supplementalfile3.html
- Supplementalfile4.xlsx